C H A P T E R - IV

X-RAY DIFFRACTION AND ELECTRON PARAMAGNETIC RESONANCE STUDIES

***

X-RAY DIFFRACTION AND ELECTRON PARAMAGNETIC RESONANCE (EPR) STUDIES

X-RAY DIFFRACTION STUDIES:

4 A-1 INTRODUCTION:

X-ray diffraction studies are used in a great variety of applications. One of the most useful and important applications of the x-ray diffraction method is the identification of solid crystalline substances. The basis of this method is the fact that each substance gives a characteristic x-ray pattern and no two chemically distinct substances give identical patterns. The positions of the lines and their relative intensities do not vary for a given experimental condition. A procedure for a quantitative analysis of the minerals has also been developed in which x-ray analysis gives results within 1 to 2 percent of chemical analysis.

The object of present investigation is -

1) To confirm the crystalline structure of the prepared CaO phosphors.
2) To obtain a possible co-relation between luminescence characteristics and structural properties.

4 A-2 Theoretical Background; Structure of CaO:

CaO possesses the cubic structure of NaCl type. The bravis lattice is face centered cubic; the basis consists of one Ca atom and one O atom separeted by one half the

body diagonal of a unit cube. There are four units of CaO in each unit cell, with atoms in the positions, Ca : o o o , $\frac{1}{2}\ \frac{1}{2}$ o, $\frac{1}{2}$ o $\frac{1}{2}$, o $\frac{1}{2}\ \frac{1}{2}$, O : $\frac{1}{2}\ \frac{1}{2}\ \frac{1}{2}$, o o $\frac{1}{2}$, o $\frac{1}{2}$ o , $\frac{1}{2}$ o o . Each Ca atom has six equidistant O atoms at nearest sites and vice versa.

4 A-2.1 Structure Determination from Powder Pattern:

The crystal structure of a substance determines the diffraction pattern of that substance; the shape and size of the unit cell determines the angular positions of the diffraction lines and the arrangement of the atoms within the unit cell determines the relative intensities of the lines. If the structure is known, its diffraction pattern can be calculated in a very straightforward manner but a direct calculation of structure from the observed pattern has never been solved. Thus the method used is essentially one of trial and error. A structure is assumed, its diffraction pattern is calculated and the calculated pattern is compared with the observed one. If the two agree in all detail, the assumed structure is correct, if not, the process is repeated as often as necessary to find the correct solution. The determination of unknown structure is complete only when the following three steps have been acomplished.

I) the angular positions of the diffraction lines are used for the deduction of the shape and size of the unit cell. The correct choice of the crystal

system, is made and correct miller indices are assigned to each reflection. This is called " Indexing the pattern ". Once the indexing is done, the shape of the unit cell is known from the crystal system and its size is calculated from the positions and miller indices of the diffraction lines.

II) the number of atoms per unit cell is then computed from the shape and size of the unit cell, the chemical composition of the specimen and its measured density.

III) the positions of the atoms within the unit cell are deduced from the relative intensities of the diffraction lines.

4 A-2.2 Idexing Powder Patterns:

The details of the procedure followed in indexing the powder patterns are described in any standard book on x-ray diffraction (1-4). Generally, the procedure involved the measurements of diffraction angle θ and correct assignment of miller indices to the observed diffraction lines. Standard charts are also available from which miller indices can be assigned directly (5,6).

4 A-2.3 Determination of Number of Atoms in a Unit Cell:

To find the number of atoms in a unit cell, use is made of the fact that the volume of the unit cell calculated from the lattice parameters multiplied by the measured density

of the substance equals the weight of all atoms in the cell. Thus -

$$\sum A = \frac{\rho V}{1.66020} \qquad \text{- - - (1)}$$

Where $\sum A$ is the sum of atomic weights of the atoms in the unit cell, ρ is the density (gram/Cm^3) and V the volume of the unit cell (A^{o3}). The volume V of the unit cell is given by -

$$V = a^3 \qquad \text{- - - (2)}$$

for the cubic unit cell and

$$V = \frac{3}{2} a^2 C \qquad \text{- - - (3)}$$

for hexagonal unit cell.

If the substance is an element of atomic weight A, then,

$$\sum A = n_1 A \qquad \text{- - - (4)}$$

Where n_1 is the number of atoms per unit cell. If the substance is a chemical compound or an intermediate phase whose composition can be presented by a simple chemical formula, then

$$\sum A = n_2 M \qquad \text{- - - (5)}$$

Where n_2 is the number of "molecules" per unit cell and M the molecular weight. The number of atoms per unit cell can then be calculated from n_2 and the composition of the phase.

The number of atoms per unit cell is always an integer, within experimental error, except for a few substences which have " defect structure".

4 A-3. Determination of Atom Positions:

To locate the positions of atoms in the unit cell use is made of the observed relative intensities of the diffracted beams, because these intensities are determined from atom positions. There is no known method of directly calculating atom positions from observed intensities and one has to proceed by trial and error.

The relative intensities of the diffracted beams are given by -

$$I = |F|^2 P \left(\frac{1 + \cos^2 \theta}{\sin^2 \theta . \cos \theta} \right) \quad - - - (6)$$

Where F is structure factor for the (hkl) reflection in terms of the atom positions (uVW) and is given by -

$$F = \sum_{1}^{N} f_n e^{2 i (hu_n + KU_n + lW_n)} \quad - (7)$$

As the relative intensity I, the multiplicity factor P and angle are known for each line on the pattern, one can find the value of $|F|$ for each reflection from equation (6). But the difficulty is that order to use equation (7) for calculating atom positions are must know the value of F, which measures both the amplitude and phase of one reflection relative to another, while $|F|$ measures only the relative

amplitude of each reflection. The intensities of the two reflated beams are proportional to the square of their amplitudes but independent of their relative phase. One can determine the intensity and amplitude but not phase and hence not the structure factor but only its absolute value can be determined. This is the reason why atom positions are determined only by trial and error. A set of atom positions is assumed, the intensities corresponding to these atom positions are calculated, and the calculated intensities are compared with the observed ones, the process being repeated until satisfactory arrangement is reached.

4 A-4. Preciese Parameter Measurements:

A precise knowledge of lattice parameter is required in many applications of x-ray diffraction. As the lattice parameter of a solid solution varies with concentration of the solute, the composition of a given solution can be determined from a measurement of its lattice parameter. In general, a change in solute concentration produces only a small change in lattice parameter and hence precise parameter measurement must be made in order to measure these quantities with any accuracy.

From the observed sin θ values of any line in an indexed cubic or hexagonal pattern, the unit cell dimensions can be determined by employing the Bragg in the forms -

$$a = \frac{\lambda\sqrt{h^2+k^2+l^2}}{2 \sin\theta} \qquad \text{--- (8)}$$

for cubic pattern.

and

$$a = \frac{\lambda}{2 \sin\theta}\left(\frac{4}{3} \cdot (h^2 + hk + k^2) + \frac{l^2}{(c/a)^2}\right)^{1/2} \qquad \text{--- (9)}$$

$$c = \frac{\lambda}{2 \sin\theta}\left[\frac{4}{3}\left(\frac{c}{a}\right)^2 (h^2 + hk + k^2) + l^2\right]^{1/2} \qquad (10)$$

for hexagonal pattern or from d spacing of any line by making use of the formula -

$$a = d\sqrt{h^2 + k^2 + l^2} \quad \text{for cubic pattern} \qquad (11)$$

and

$$a = d\left[\frac{4}{3}(h^2 + hk + k^2) + \frac{l^2}{(c/a)^2}\right]^{1/2} \qquad \text{--- (12)}$$

$$c = d\left[\frac{4}{3}\left(\frac{c}{a}\right)^2 (h^2 + hk + k^2) + l^2\right]^{1/2} \qquad \text{--- (13)}$$

for hexagonal pattern.

In case of cubic system, theoretically true value of 'a' is obtained simply by plotting the measured values against 2 θ and extrapolating to 2 $\theta = 180^{\circ}$. But this curve is not linear and hence the measured values of 'a' must be plotted against some function of θ . In practice, a best value of 'a' is to be obtained by plotting measured values of 'a' against $\sin^2\theta$ or $\cos^2\theta$ (7). If various sources of errors are analysed more rigorously the measured values

of 'a' are plotted against $\frac{1}{2}\left(\frac{\cos^2\theta}{\sin\theta}+\frac{\cos^2\theta}{\theta}\right)$ and this holds quite accurately down to very low values of θ.

In case of non-cubic systems, the values of 'a' are obtained from each (hko) lines and those of 'c' from each (001) lines. Two separate extrapolations are then used to find the correct values of 'a' and 'c'. Since there are very few (hko) and (001) lines in the back reflection region, some low angeled lines have to be included which means that the extrapolation must be made against $\frac{1}{2}\left(\frac{\cos^2\theta}{\sin\theta}+\frac{\cos^2\theta}{\theta}\right)$ and not against $\cos^2\theta$ or $\sin^2\theta$.

A better but laborious method is that of successive approximation. The approximate values of 'a_1' and 'c_1', are calculated from the positions of the two highest angled lines. The approximate axial ratio (a_1/c_1) is then calculated and used in equation (9) to determine 'a' value for each high angled line on the pattern. These values are then extrapolated against $\cos^2\theta$ to find a more accurate value of 'a' namely a_2. The value of c_2 is then found in similar manner by the use of relations (eqn.19) and another extrapolation against $\cos^2\theta$. The process is repeated with new axial ratio (a_2/c_2) to give still more accurate values of the parameters. Three extrapolation are usually sufficient to fix the parameters with high accuracy.

4 A-5 Qualitative Analysis of Powder Mixtures:

Powder x-ray diffraction analysis is the perfect technique for crystalline mixture analysis, since each component of the mixture produces its characteristic pattern independently of the others. Moreover, the intensity of each component's pattern is proportional to the amount present, except for an absorption correction. Hull (8) pointed out these unique features of the powder pattern but the technique was successfully used by Clark and Reynolds (9) for mine-dust analysis. Following Clark and Reynolds, Brentano (10) discussed theoretically the measurements of the absolute intensities of x-rays diffracted by the components of a binary powder mixture. In a similar manner, Glocker (11) and Schafer (12) showed that the fundamental intensity formulae of Laue could be applied in the quantitative diffraction analysis of binary powder mixtures and alloys. However, a simple but important mathematical relationships between pattern intensity and the absorptive properties of the sample were little investigated until Alexander and Klug (13) developed a systematic practical scheme of analysis.

Alexander and Klug's formula takes a simplified form when applied to a mixture of two components (binary mixture). For the pure component 1

$$\left(I_{i1} \right)_0 = \frac{K_{i1}}{\varrho_1 \mu_1} \qquad \text{- - - (14)}$$

and for a binary mixture with a weight fraction X_1 of this component -

$$I_{i1} = \frac{K_{i1} X_1}{\rho_1 (X_1 (\mu_1 - \mu_2) + \mu_2)} \qquad \text{- - - (15)}$$

Here K_{i1} depends upon the nature of component 1 and the geometry of the apparatus, I_{i1} is the intensity of line i of pure component 1, S_1 in the density of the solid component 1 and μ_1 and μ_2 are the mass absorption coefficients of components 1 and 2 respectively. Division of equation (15) by equation (14) gives the expression for theoretical analysis:

$$\frac{I_{i1}}{(I_i 1)_o} = \frac{X_1 \mu_1}{X_1 (\mu_1 - \mu_2) + \mu_2} \qquad \text{- - - (16)}$$

If $\mu_1 = \mu_2$, the weight component of X_1 component is directly proxortional to the intensity ratio $I_{i1} / (I_i 1)_o$. It is evident from equation (16) that the intensity ratio is greater than X_1 when $\mu_1 > \mu_2$ and less than X_1 when $\mu_1 < \mu_2$.

4 A-6 RESULTS AND DISCUSSION:

4 A-6.1 Fluxed CaO, CaO:Bi and CaO:Sm phosphors:

In fig.4.1 is shown a diffraction pattern of CaO with flux ($Na_2 S_2 O_3$, $Na_2 SO_4$, Na F). The diffraction pattern of fluxed CaO gives number of broad lines, indicating thereby the sample (S_o) is crystalline in nature. Lehmann (14) has

reported that CaO crystallizes in the same cubic NaCl lattice as CaS. Thus, the peak of maximum height is assigned to a value of h k l = 3 1 1 and indexing of rest of the lines is made according by taking the value of lattice parameter a = 8.71 Å. The value of 'a' is in agreement with that given by the relation -

$$d_{200} : d_{220} : d_{111} = \frac{a}{2} : \left(\frac{1}{2\sqrt{2}}\right)a : \left(\frac{1}{\sqrt{3}}\right)\times a$$ for FCC (15). The 'd' values calculated are in good agreement with the observed ones. The results obtained are summarised in table 4.1. The h k l values assigned to each reflected line show that the structure is face centered cubic. Some other lines also occur at low angle which might be due to perturbations in the lattice because of flux (16).

Fig.4.2 shows the diffraction pattern of fluxed CaO:Bi. Indexing of the reflected lines is done by the same method as above and it has been found that the sample is face centered cubic. Some additional lines are also observed as that for sample(S_o) and these might be due to the addition of flux. The observed and calculated 'd' values agree well. On comparision of a XRD of sample S_o (fig.4.1) (CaO with flux) with that for sample S_6 (fig.4.2) (CaO:Bi with flux) a decrease in peak heights for sample S_6 is observed indicating thereby the number of atoms in a plane decrease with addition of Bi^{3+}. This is since intensity is directly proportional to the concentration of atoms in a plane. It is also found that there is a very small

shift in the line positions towards the higher angle side suggesting thereby a decrease in lattice parameter 'a'. However, the observed change is too small.

Fig.4.3 shows the diffraction pattern of a fluxed CaO;Sm phosphor. Indexing of the lines results in face centered cubic structure. As before here also additional lines are observed and we attribute these to the flux. The calculated and observed 'd' values agree well. A comparision of XRD of fluxed CaO:Sm with that of sample CaO with flux gives same results as that obtained for CaO;Bi with flux. The positions of lines shifts towards higher angle side with decrease in peak heights. The observed value of lattice constant 'a' is less than that observed for fluxed CaO('a' for fluxed CaO = 8.71 $\AA^{o}$ and for fluxed CaO:Sm = 8.69 $\AA^{o}$).

From above results one can conclude that:

1) CaO, CaO:Bi and CaO:Sm crystallize in face centered cubic lattice.
2) Incorporation of Bi^{3+} and Sm^{3+} results in decrease in the peak height suggesting thereby the number of atoms in a plane decrease.
3) Incorporation of Bi^{3+} and Sm^{3+} causes to reduce lattice constant but the observed change is very small. It will be worth mentioning that we attributed the additional lines observed in XRD of studied samples to the presence of flux

and not to the $CaCO_3$ which might be suspected to be present in a prepared phosphors due to the incomplete reduction of $CaCO_3$ into CaO. This is since, $CaCO_3$ has rhombohedral. Crystal structure and observed lines do not correspond to such a structure.

4 B: ELECTRON PARAMAGNETIC RESONANCE STUDIES

4 B-1 INTRODUCTION:

Electron paramagnetic resonance (EPR) is a branch of absorption spectroscopy in which radiation of microwave frequency is absorbed by unpaired electrons in a magnetic field. It was first reported and was used successfully for the study of Zeeman levels in paramagnetic substances by Zavoisky (17). Later it was extensively developed by Bleaney et.al (18) and many others(19-21).

Electron paramagnetic resonance requires the presence of unpaired electron and hence a resultant angular momentum in the system to be studied. Such an electron paramagnetism is found in all atoms having an odd number of electrons, in ions having partly filled inner shells, in molecules having odd no.of electrons such as NO, in free radicals, in colour centres such as electrons or holes trapped in various regions of lattices of crystals due to irradiation, in metals and semiconductors caused by conduction electrons.

The resonance technique is particularly useful for the study of semiconductors, electrical, optical and other proporties of semiconductors are extremely sensitive to small concentrations of impurities and the advantage of E P R is its extreme sensitivity to very small amount of paramagnetic materials. Under favourable conditions a signal for diphenylpicrylhydrazyl (DPPH) redical can be detected if there are 10^{-12} gram of material in the spectrometer. The resonance properties of some imperfections, notably the shallow donor or shallow acceptors, are determined largely by the band structure of the host lattice. Valuable information about the band structure has also been obtained from resonance studies.

The present E PR measurements are carried out with a view:

1) to obtain the information about the nature and origin of paramagnetic defects responsible for luminescence centres and traps, and;

2) to see the effect of changing the percentage of the activators Bi and Sm and of both combiningly on the general feature of E PR spectra.

4 B-2 THEORETICAL BACKGROUND:

4 B-2.1 Resonance Conditions:

In a magnetic field H, the energy levels of a free paramagnetic ion having a resultant angular momentum J are given by:

$$E = g \beta H M \qquad \text{- - - (17)}$$

Where $\beta = (eh/ 4\pi mc)$ is the Bohr magneton, M, the projection of J along H, ranges from +J to -J in integral steps. The 'g' factor, known as Lande's g factor, is given by

$$g = 1 + \frac{J(J+1) + S(S+1) - L(L+1)}{2J(J+1)} \qquad \text{- - -(18)}$$

Where S and L are the electron spin and orbital angular momentum vectors, respectively. If an alternating field of frequency ν is applied perpendiculer to H, magnetic dipole transitions are produced. The selection rule for the magnetic dipole transitions is $\Delta M = \pm 1$. Thus the photons which are resonantly absorbed are those where energy is equal to the separation between adjacent energy level i.e.

$$h\nu = g \beta H \qquad \text{- - - (19)}$$

The g value is a characteristic of a particular spin system. For a completely free electron (ion) g has a value of 2.0023. But in practice it can not be conceived free electron because it is associated with ions and moleculas and as a result electron is couple to their orbital motion . Thus the 'g' value is a measure of the spin and orbital contributions to the total magnetic moment. Therefore, any devation of the 'g' value can be attributed to the spin orbit interaction.

4 B-2.2 Fine Structure:

The strong electric field produced by the dimagnetic neighbours around the paramagnetic ion causes a stark splitting of the energy levels. The amount and the nature of the splitting strongly depends upon the nature of the crystal field around the ion. Consequently, the behaviour of the paramagnetic ion in a crystal is obtained from the stark splitting of the free ion levels in the crystalline electric field. Because of the asymmetric crystal field, the contribution from the orbital motion is anisotropic. The 'g' values obtained are also anisotropic whenever there is any contribution from the unquenched orbital angular momentum. When the paramagnetic ion is in the vicinity of a nucleus with a nonzero molecular spin I, an interaction takes place which causes the absorption signal to split into 2 I + 1 components. The cause of this hyperfine splitting in an isotropic system is the nuclear spin-electron spin coupling arising mainly from Fermi contact term. From a fully resolved EPR spectrum the 'g' values and the hyperfine splitting constants can be determined with great accuracy which in turn provide the information about the electronic states of the unpaired electron and also the nature and bonding of the paramagnetic ion with its diamagnetic neighbours. This aspect has been extensively studied in the transition group elements. Bethe and Van Vleck have successfully interpreted the magnetic properties using the

crystal field theory. But the 'g' values obtained experimentally are found to be lower than those predicted from the crystal field theory (18,19). This discrepancy of the difference of 'g' values has been successfully explained by introducing the covalency in the metal ligand bonding, whereas in the crystal field theory it is purely ionic. In the modified theory (ligand field theory) the main features are -

a) a reduction in the oribtal contribution to the 'g' values,

b) an increase in the spin lattice relaxation, and;

c) an observation of superfine structure.

4 B-2.3 General Hamiltonian of the "Free Ion":

An unpaired electron in a crystal is subjected to the most complex interacting field. This state of affairs can be conveniently expressed from the quantum mechanical view point in terms of Hamiltonian. Abragam and Pryce initially and other numerous workers subsequently described the electronic interactions which contribute to the total energy of the ion by the following Hamiltonian:

$$H = H_C + H_{Cr} + H_{S-O} + H_{S-S} + H_Z + H_{hf} + H_Q + H_n + H_e \quad --(20)$$

The terms for the free ion have been listed in the order of describing magnitude. The significance of the terms and their order of effect on the free ion have been given below:

H_C - free ion or coulomb energy, 10^5 Cm^{-1}.

H_{Cr} - stark crystalline or electrostatic field, 10^4 Cm^{-1}.

H_{S-O} - electronic spin orbit interaction energy, 10^2-10^3 Cm^{-1}.

H_{S-S} - electronic spin-spin interaction energy, 1 Cm^{-1}.

H_Z - Zeeman energy interaction of the electron with the magnetic field= $\beta H (L+2S)$ 1 Cm^{-1}.

H_{hf} - Dipole-dipole coupling between the electron nuclear magnetic moments, 10^{-1}-10^{-3} Cm^{-1}.

H_Q - Quadrapolar or higher electrostatic interaction between the electron and the nucleus, 10^{-3} Cm^{-1}.

H_n - Nuckar Zeeman energy interaction of the nucleus with the external magnetic field= $g_1 \beta_1 M I$, 10^{-4} Cm^{-1}.

H_e - energy of exchange effect between two types of electrons.

All the contributions listed above are not significant because the energy contribution from various terms ranges over a wide frequency and some interactions fall outside the realm of E P R. H_C , H_{Cr} and H_{S-O} involve too much energy for excitation of E P R while H_Q , H_n and H_e are frequently too small to observe in the presence of H_Z consequently, the fine structure, the Zeeman splitting and hyperfine structure are the main concerns of the E P R spectroscopy because they involve energies ideally suited to the existing microwave practice.

Calculations with the total Hamiltonian are very difficult and, therefore, a simplified accounting of the more likely interactions is performed with a spin Hamiltonian developed by Abragam and Pryce and other workers. The spin Hamiltonian given below is used to give shorthand description of the experimental results. The hyperfine constants, 'g' factors and zero field splitting are determined experimentally and these are fitted to models with the aid of the Hamiltonian. The spin Hamiltonian for a principal axis system can be written as -

$$H = D S_Z^2 - \frac{S\,(S+1)}{3} + E\,(S_x^2 - S_y^2) + \beta\,(g_x S_x H_x + g_y S_y H_y + g_z S_z H_z) + A_z I_z S_z + A_x I_x S_x + A_y I_y S_y + Q\left(I_z^2 - \frac{I\,(I+1)}{3} - g_I \beta_I H I\right) \qquad \text{- - - (21)}$$

Where S is the effective spin, β and β_I are the Bohr and nuclear magnetons and g's are the splitting factors, I being the nuclear spin and D, E, A, Q, the interaction coefficients.

If the crystalline electric field possesses an axial symmetry (tetragonal, trigonal or hexagonal), the various tensors are characterised by the principal values one along and other perpendicular to the symmetry axis (Say Z axis).

$$g_z = g_{11}\,, \qquad g_x = g_y = g_1$$

$$A_z = g_{11}\,, \qquad A_x = A_y = A_1$$

and $$S_x^2 = S_y^2$$

and the spin Hamiltonian can be simplified as

$$H = D\left(S_z^2 - \frac{S\,(S+1)}{3} \right) + \beta - g_{11} S_z H_z + g_1 (S_x H_x + S_y H_y) +$$

$$A_{11}\, I_z\, S_z + A_1 \left(I_x S_x + I_y S_y \right) \qquad - - - \ (22)$$

This equation is of great significance in E PR of the crystalline state.

H_y fitting the experimentally observed spectrum into the above expression representing the lowest energy level it is possible to determine the numerical values of the different constants occuring in the Hamiltonian and these in turn can be used to obtain some information regarding the symmetry of the crystalline electric field and the environment of the paramagnetic ion in the crystalline state.

4 B-2.4 E P R Spectrum of M_n :

M_n^{2+} typically has a half filled 3d shell. The configuration is $3d^5$ and the ground state of free ion is 6S. Its spin degeneracy is known to split, under the combined effect of an externally applied magnetic field and a crystallined field, according to the spin Hamiltonian.

$$H = \beta H g \quad S + D \left(S_z^2 - \tfrac{1}{3} S(S+1) \right) + \beta \left(S_x^2 - S_y^2 \right) +$$

$$F(a) + A S_z I_z + B \left(S_x I_x + S_y I_y \right) - \nu \beta_n H \quad I +$$

$$Q \left(I_z^2 - I \frac{(I+1)}{3} \right) \qquad \text{- - - (23)}$$

Here g is the spectroscopic splitting factor, β is the Bohr magneton, H is the external magnetic field, S is the total spin operator and I is the nuclear spin operator. The first term represents the Zeeman effect and the next three terms represent the fine structure interaction induced by crystalline field. Of the total crystalline field the D term shows the effect of the axial symmetric part, while E and F terms represent the effects of rhombic and cubic parts respectively.

The last four terms of the Hamiltonian are these involving the spin I of manganese nucleus (M_n^{55}), which produces a hyperfine structure. The A and B represent the interaction between the magnetic field of the electron and the magnetic moment of the nucleus. Axial symmetry is assumed in writting the same coefficients for X and y components. The remaining terms are too small to produce an observable effect on the spectrum.

The energy level diagram of $M_n^{2+}(d^5)$ is illustrated schematically in fig. 4.3*a*. In the absence of any nuclear effects and in zero magnetic field, the six-fold electronic

state is split, into three doublets by electronic magnetic interaction, with separation of 4D and 2D. When a strong magnetic field is applied parallel to the axis of symmetry (Z-axis) all the degeneracy is lifted and successive levels are separated by G+4D, G, G-2D and G-4D respectively. Since the selection rule allow M to change by ± 1, the spectrum would consist of five equally spaced lines corresponding to these separations. If the nuclear interaction is now introduced each level is split up into six components, each corresponding to one of the $(2I + 1)$ orientations which the nuclear spin takes up in the very high magnetic field of its surrounding electron cloud. The spacing within each sextuplate is constant, and proportional to the magnetic quantum number of the electronic level. Since the applied oscillating magnetic field has a negligible interaction with the nuclear moment, the only allowed transitions are those involving no change in the nuclear orientation ($\Delta m = o$). Thus each electronic transition is split into six equally spaced hyperfine components.

4 B-3 RESULTS AND DISCUSSION:

4 B-3.1 EPR Spectrum of CaO Phosphor (With Flux):

Fig.4.4 shows the typical EPR spectrum of CaO phosphor with flux. In this sample the characteristic M_n^{2+} spectrum is observed. M_n has not been added intentionally

as an activator but it might be present as a trace impurity. It has been reported that M_n^{2+} is extremely, sensitive to E P R measurements and an observable spectrum can be obtained even if 10^{-11} mole of it is present in cubic crystal field (22). In the above spectrum of CaO, the six characteristic M_n^{55} hyperfine lines corresponding to the transition $M = +\frac{1}{2} \rightarrow -\frac{1}{2}$ are observed. In addition to these six lines some other lines corresponding to other allowed transition and forbidden transitions are also observed in the spectrum. Such E P R spectrum of M_n , as a trace impurity, has also been observed by Shankar et.al (23) and Hadgal R.R.(24) in CaS phosphors.

The above results thus indicate that M_n^{2+} is present as a trace impurity in CaO phosphr and is probably introduced through the starting materials used in the preparation of the phosphors.

4 B-3.2 E P R Spectra of CaO:Bi Sm Phosphors:

Figs.4.5 and 4.6 show the typical E P R spectra of Bi^{3+} doped samples along with E P R spectrum of undoped CaO phosphor. All the samples, doped as well as undoped exhibit similar nature consisting of six strong hyperfine lines along with same lines of other allowed transitions and forbidden transitions. The six strong lines are the characteristics M_n^{55} lines for the transitions $M = \frac{1}{2} \rightarrow -\frac{1}{2}$. No signal corresponding to Bi^{3+} was observed because Bi^{3+} is to be

detected only at low temperatures (below 20°K) (25-27). Moreover, as Mn^{55} is very sensitive to E P R measurements, other impurities and defects cannot be detected in its presence. One more inference which can be drawn from the above E P R spectra is that, addition of Bi^{3+} does not change notably the crystal field surrounding the Mn^{2+} ion.

Figs.4.7 and 4.8 show the E P R spectra of some samples doped with Sm^{3+} as an activator. For all these samples, the same six hyperfine lines of Mn^{55} corresponding to the transitions $M = +\frac{1}{2} \rightarrow -\frac{1}{2}$ are observed. The lines corresponding to other allowed transitions and forbidden transitions are not seen in the spectrum.

It is evident from the above results that addition of Sm^{3+} changes the crystal field surrounding the Mn^{2+} ion and suppresses the allowed and forbidden transition except the transitions corresponding to $M = +\frac{1}{2} \rightarrow -\frac{1}{2}$. No signal corresponding to Sm has been observed since as stated earlier impurities and defects in presence of Mn^{2+} is not feasible.

In figs.4.9 and 4.10 are shown the E P R spectra of samples doped with Bi^{3+} and Sm^{3+} simultaneously. All these samples exhibit similar nature consisting of six hyperfine lines of Mn^{55} corresponding to the transitions $M = +\frac{1}{2} \rightarrow -\frac{1}{2}$. The general feature of the spectra is

similar to that for CaO;Sm phosphors. From these results one can conclude that when Bi^{3+} and Sm^{3+} are added simultaneously, Sm^{3+} plays a major role in changing the crystal field surrounding the M_n^{2+} ions.

4 B-3.3 Spin Hamiltonian Parameters:

As the E P R investigation were carried out on powder samples, it enabled only the hyperfine constant 'A' and spectroscopic splitting factor 'g' to be measured (28). For this measurements, the transitions $M = +\frac{1}{2} \rightarrow -\frac{1}{2}$ is used. The spin Hamiltonian parameters are listed in table 4.2.

The average Hyperfine structure constant is found to be 89.9 Gauss for CaO, 90.28 Gauss for CaO:Bi, 85.7 Gauss for CaO:Sm and 85.5 for CaO:Bi:Sm samples. The value of ' 'g' varies between 1.99921 to 2.00277 and the variation is unsystematic in nature. The line width for CaO is found to be 6 Gauss, for CaO:Bi phosphors it changes from 6.25 to 7.66 Gauss, for CaO:Sm phosphors it changes from 1.66 to 3.5 Gauss and for CaO:Bi:Sm phosphors it changes from 1.75 to 2.0 Gauss. But these changes are unsystematic in nature.

4 C. SUMMARY:

The principal findings of this chapter may be summarised as below:-

1) CaO prepared by thermal reduction shows a face centered cubic structure with lattic constant 8.71 A°.

2) Incorporation of Bi^{3+} and Sm^{3+} into CaO results in decrease in peak heights suggesting thereby number of atoms in a plane is reduced.

3) Addition of Bi^{3+} and Sm^{3+} found to reduce lattice constant but the observed effect is very small.

4) M_n^{2+} is present as a trace impurity in the prepared $CaO:Bi;S_m$ phosphors.

5) A change in percentage of Sm^{3+} changes the crystal field surrounding the M_n^{2+} ions. But no such change has been observed for Bi^{3+}.

6) No signal corresponding to activators Bi^{3+} and Sm^{3+} is observed.

7) There is no significant and systematic change in the 'g' values.

-oo-

Table No.4.1: X-ray diffraction data and d values for CaO, CaO:Bi and CaO:Sm phosphors.
(a = 8.71 $\AA^{o}$ for S_o S_6 and a = 8.69 $\AA^{o}$ for S_{16})

Sample No.	h k l	d_{obs} $\AA^{o}$	d_{Cal} $\AA^{o}$
	111	4.9279	4.92805
	220	3.1104	3.11029
	311	2.6292	2.62917
S_o	420	1.9294	1.92939
	422	1.7972	1.79719
	511,333	1.6865	1.68648
	531	1.4796	1.47961
	600,442	1.4507	1.45069
	622	1.3147	1.31468
	111	4.9009	4.90108
	220	3.0789	3.07888
	311	2.6292	2.62917
	420	1.9065	1.90654
	422	1.7939	1.79393
S_6	511,333	1.6808	1.68077
	531	1.4817	1.48171
	600.442	1.4467	1.44665
	622	1.3147	1.31468
	111	4.9279	4.92805
	220	3.0998	3.09961
S_{16}	311	2.6217	2.62171
	420	1.9255	1.92554
	422	1.7906	1.79063
	511,333	1.6836	1.68362
	531	1.4796	1.47961
	600,442	1.4487	1.44865
	622	1.3099	1.30994

Table No.4.2: Spin Hamiltonian Parameters:

Sample No.	'g'	Hyperfine Structure constant A in Gauss	Line Width in Gauss
S_o	2.00277	89.9	6.00
S_2	1.99921	89.7	6.25
S_4	1.99978	87.1	6.63
S_6	2.00127	92.4	6.66
S_8	2.00127	90.9	7.66
S_{10}	2.00098	91.1	7.66
S_{12}	2.00211	86.2	3.5
S_{14}	2.00247	86.2	2.16
S_{16}	2.00247	85.3	2.16
S_{18}	2.00203	85.4	1.66
S_{20}	2.00217	85.4	1.66
S_{21}	2.00203	85.5	2.00
S_{23}	2.00173	85.5	1.83
S_{25}	2.00203	85.6	1.75

REFERENCES

1. Klug,H. and Alexander,L. " X-ray Diffrection Progress for polycrystalline and Amorphous Materials" (John Wiley and Sons, New York,1974).

2. Clark,G.L, " Applied X-rays" (Mc Graw Hill Book Company, Inc.,New York, 1955).

3. Azaroft,L.V. " Elements of X-ray Crystallography" (Mc Graw Hill Book Company, New York,1968).

4. Cullity,B.D." Elements of X-ray Diffraction", Addison-Wesley, Reading, Massachusetts 1956).

5. Hull,A.W. and Devey,W.P., Phys.Rev.,17,549 (1921).

6. Davey,W.P., Gen.Elec.Rev.,25, 564 (1922).

7. Bradley,A.J. and Jay,A.H., Proc.Phy.Soc.(London), 44, 563 (1932).

8. Hull,A.W., J.Am.Chem.Soc.,41, 1168 (1991).

9. Clark,G.L. and Reynolds, D.H.,Ind.Eng.Chem.Anal. Ed.8, 36 (1936).

10. Brentano,J.C.M., Phil.Mag.(7), 6, 178 (1928); Proc.Phys.Soc.(London), 47, 932 (1935).

11. Glocker,R.,Matallwritschaften,12,599 (1933).

12. Schafer,K.Z., Kristallogr, 99, 142 (1938).

13. Alexander,L. and Klug,H.P., Anal.Chem.20,886 (1948).

14. Lehmann,W.J., Luminescence, 6 (1973), 455.

15. George,M.V., Mahanty,J.,P.T.Narsimhan and Rao,C.N.R., "A Hand Book of Chemistry and Physics".

16. Larach,S. and Turkerich,J., Phys.Rev.,98,1015 (1955).

17. Zavoisky,E.J.J., Phys.(VSSR), 9,211 (1945).

18. Bleaney,B. and Stevens, K.W.H., Repts.Proger in Phys., 16, 108 (1953).

19. Bowers,K.D. and Owen,J., Repts.Proger in Phys., 18, 304 (1955).

20. Orton,J.W., Repts. Proger, in Phys.,22,204 (1959).

21. Low,W., " Solid State Physics", Suppl.2 (1960).

22. Hershberger,W.D. and Lietor,H.N., Phys.Rev.,88,714 (1952).

23. Shankar,V., Ghosh,P.K. and Reddy,T.R., Indian J. Pure Appl.Phys.,14, 193 (1976).

24. Hadgal,R.R., Ph.D.Thesis,Shivaji University,Kolhapur,1982.

25. Smith,G.E., Gatt,J.K. and Merritt,F.E.,Phys.Rev. Letters, 4, 276 (1960).

26. Beleaney,B., Tech.Rept.,AFCRI 63-192 (1963).

27. Watts,R.K. and Hotton,W.C., " International Conference on II-VI Semiconducting Compounds", New York, Dec.1967, p.1390.

28. Awate,A.V., Ph.D.Thesis,Shivaji University,Kolhapur,(1975).

-oo-

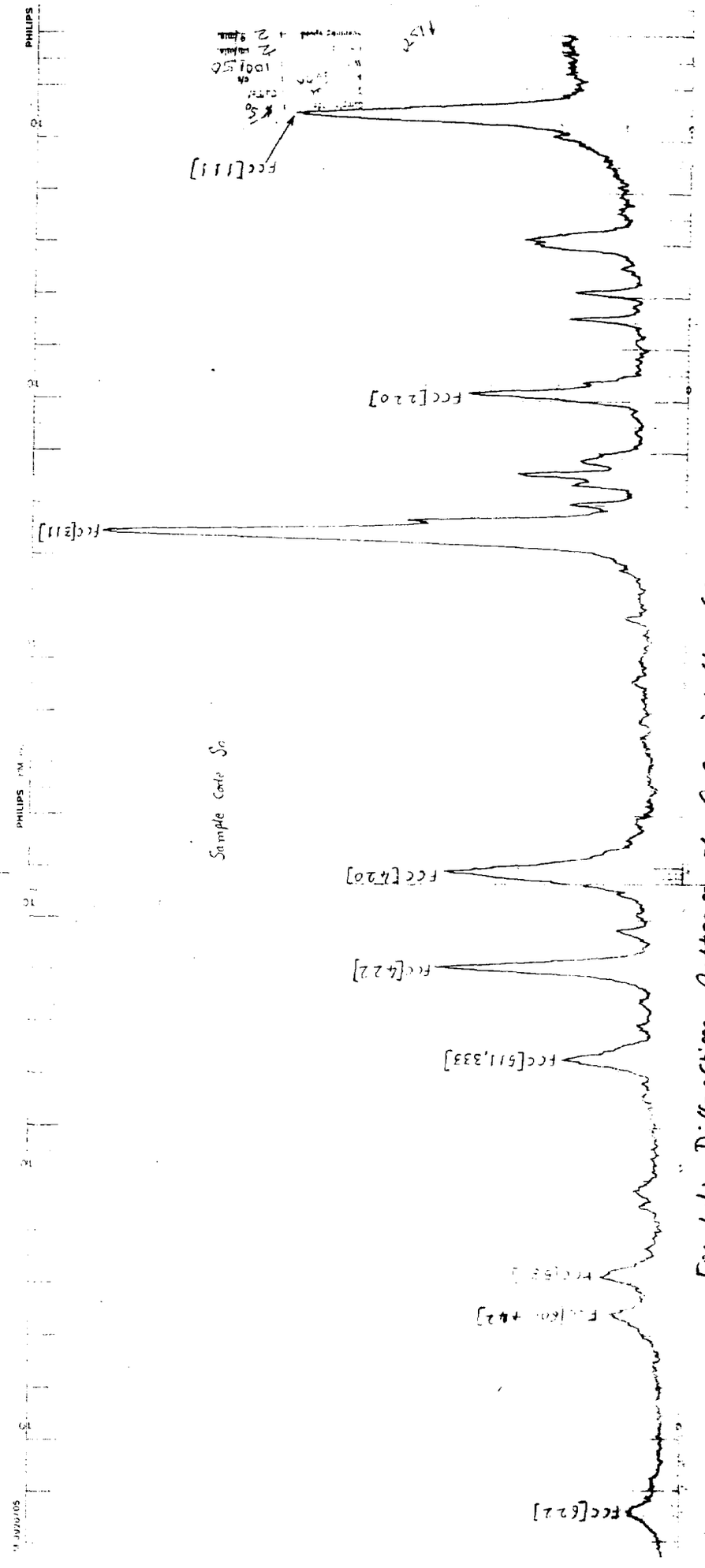

Fig. 4·1: Diffraction Pattern of CaO with flux (So)

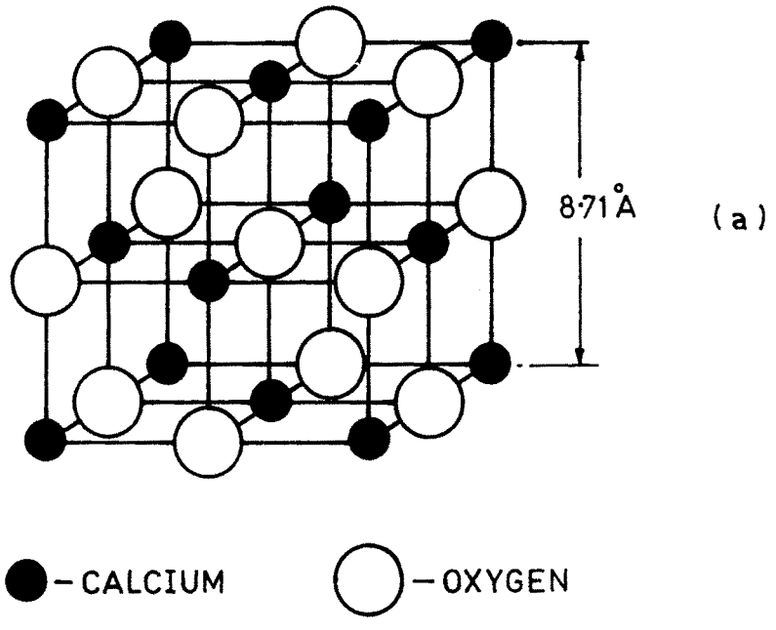

FIG. 4·1 (a): CRYSTAL STRUCTURE OF CaO

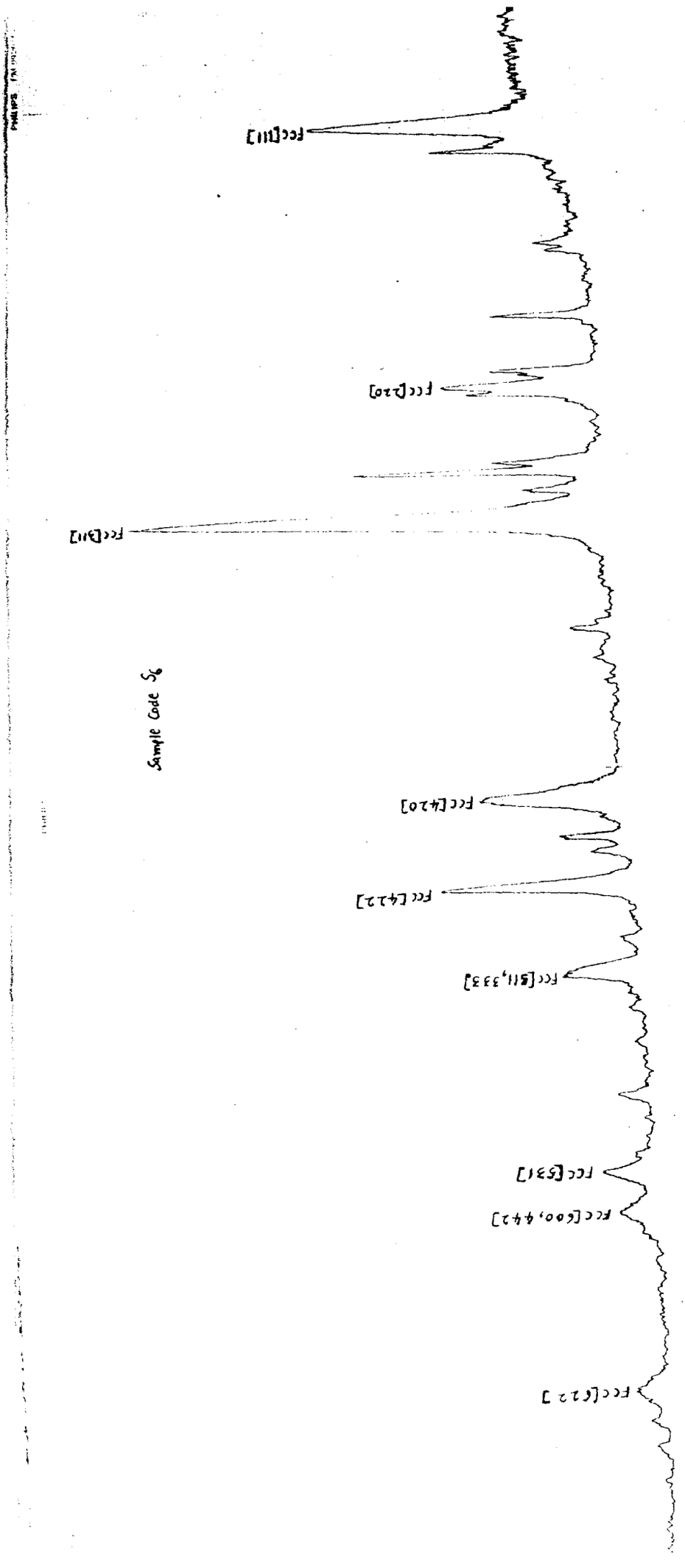

Fig. 4.2: Diffraction pattern of CaO: Bi with Flux (S6)

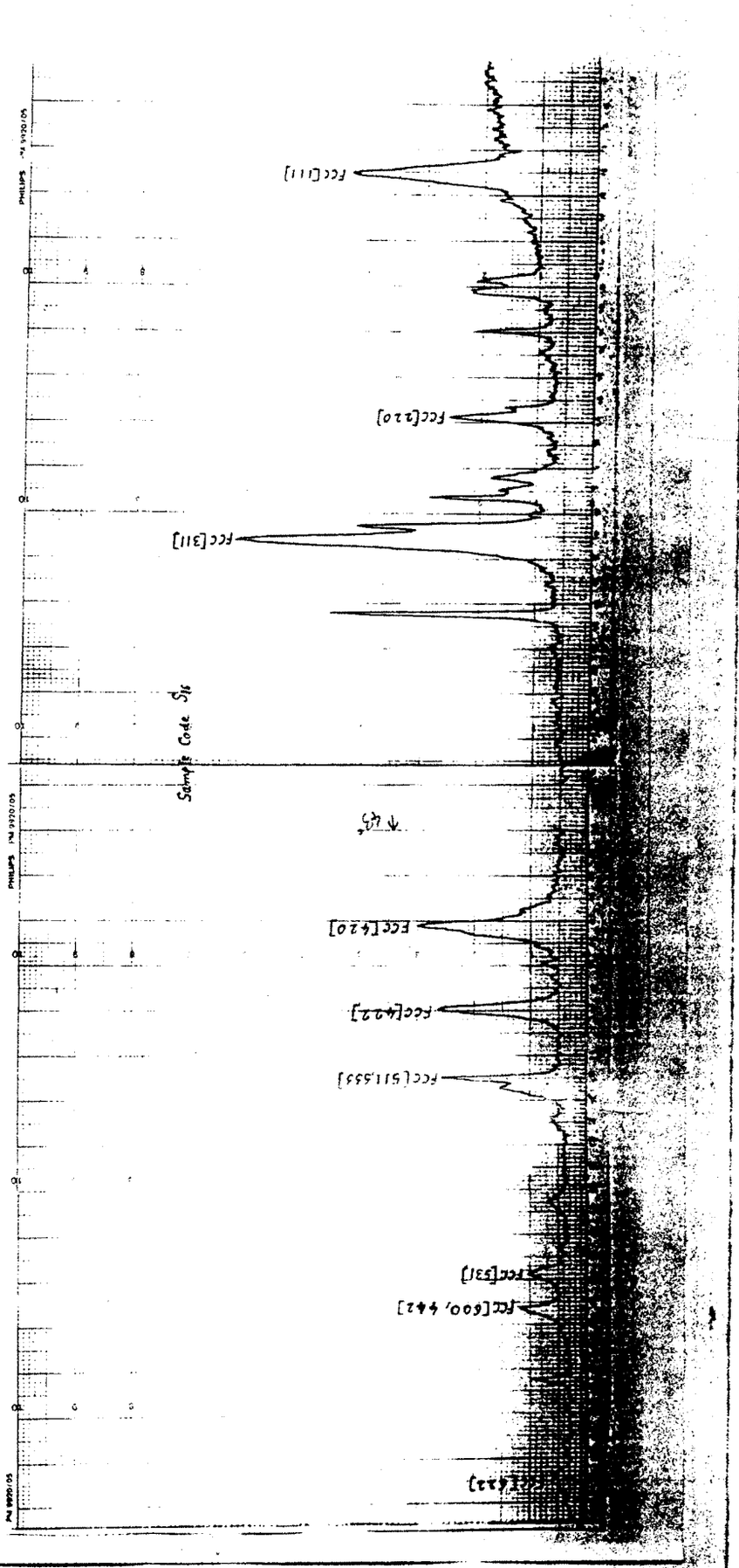

Fig. 4.3: Diffraction Pattern of CaO:Sm with flux (S16)

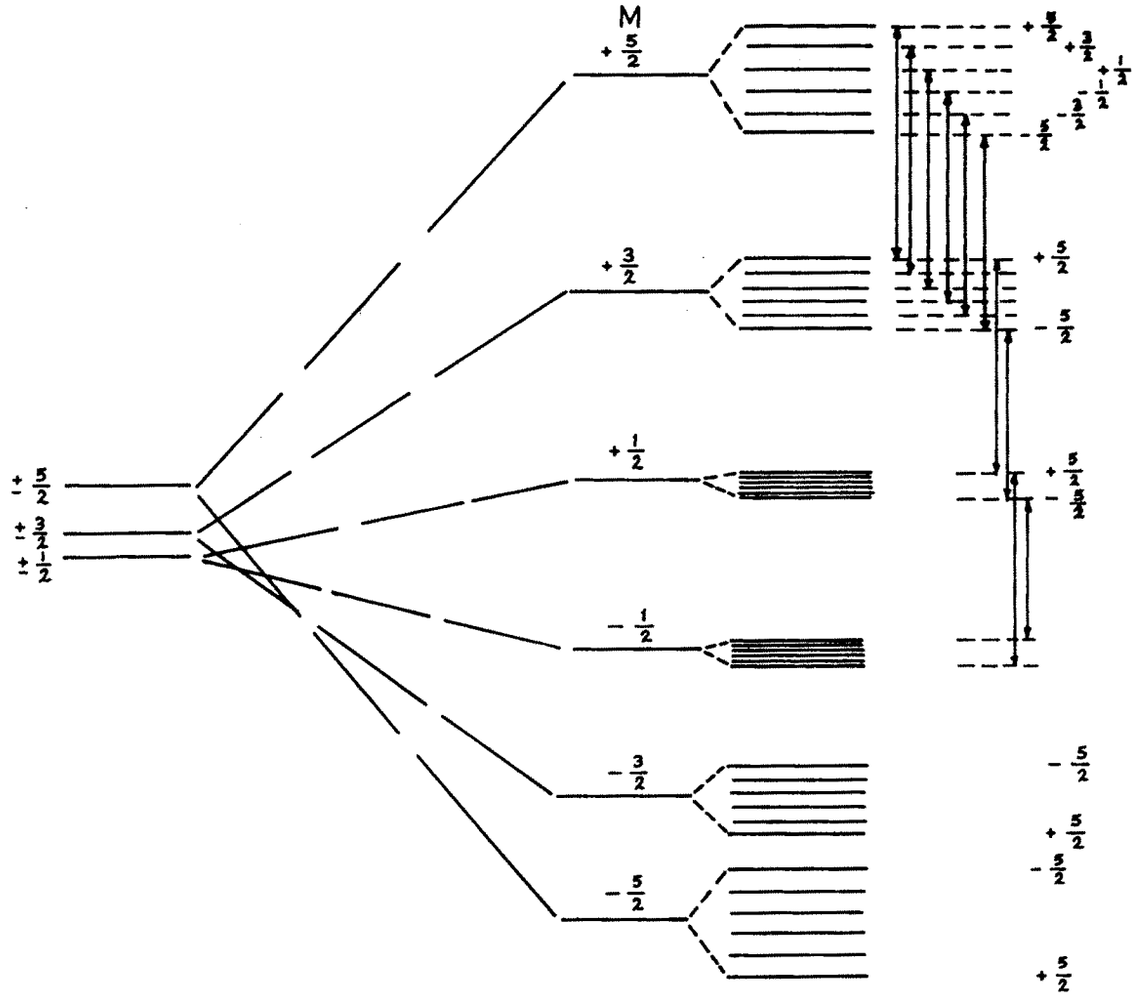

FIG. 4·3a ENERGY LEVEL DIAGRAM OF $Mn^{2+}(d^5)$

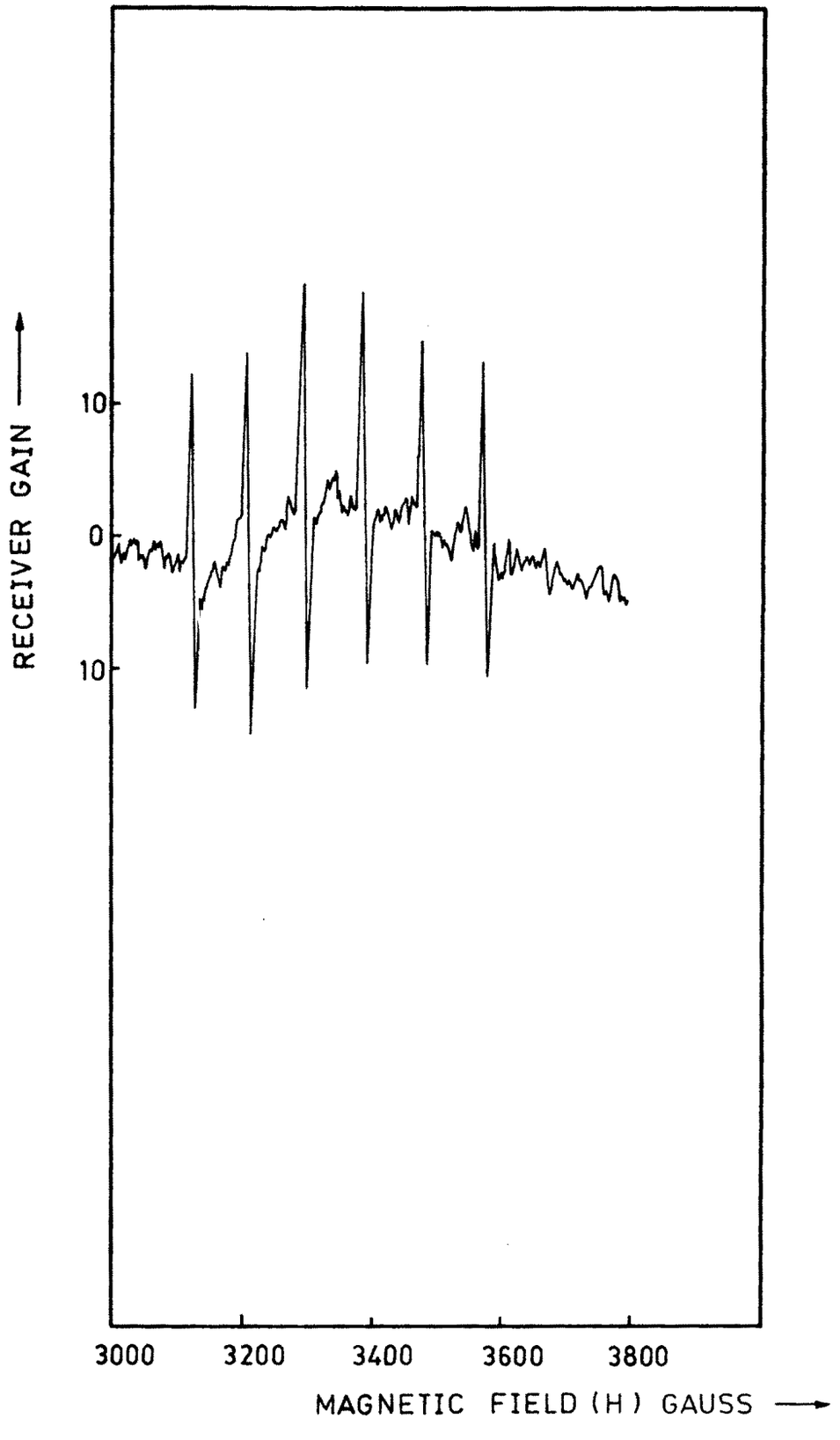

FIG. 4.4 EPR SPECTRA OF FLUXED CaO PHOSPHOR (S_0)

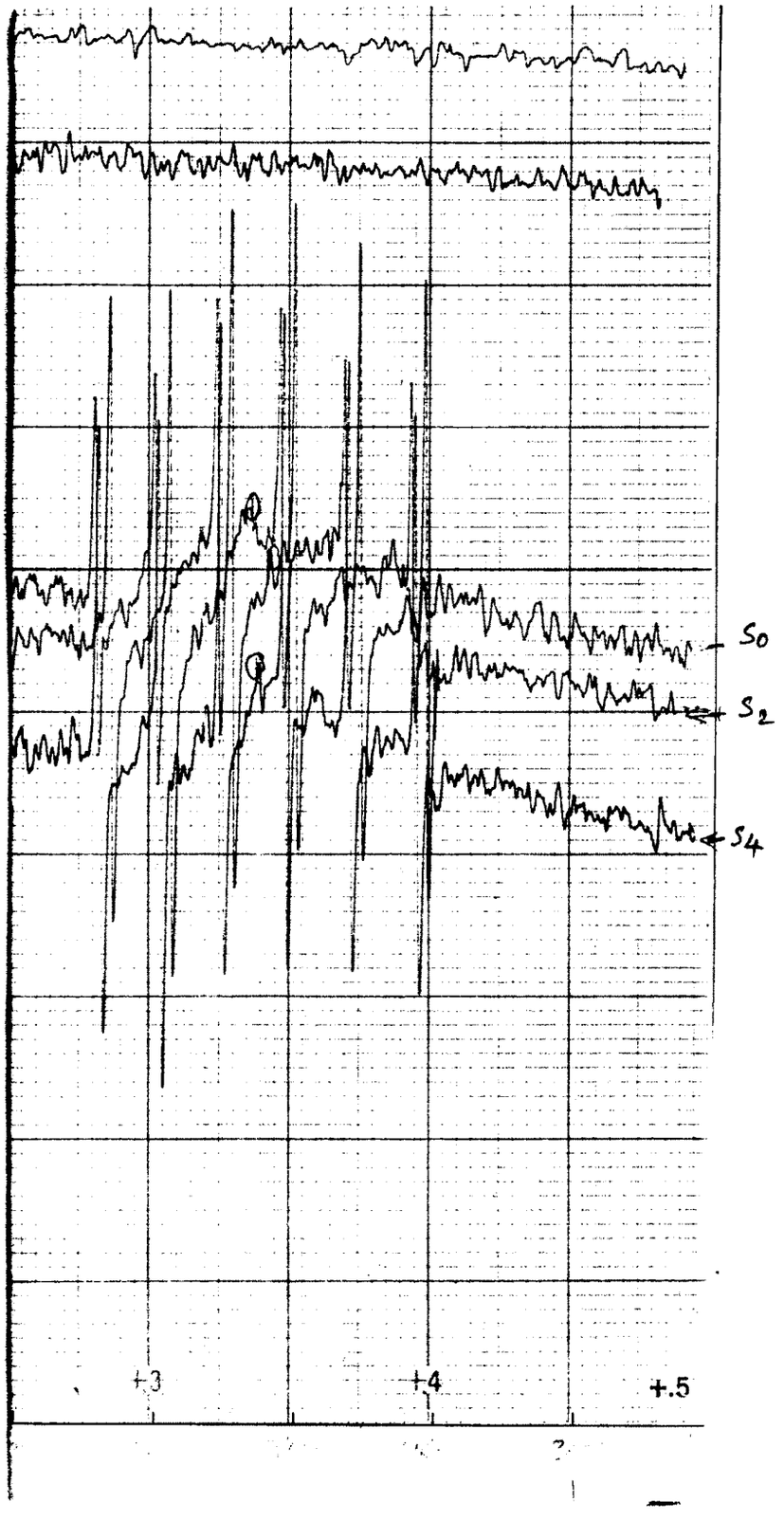

Fig. 4.5: EPR Spectra of fluxed CaO: Bi phosphors.

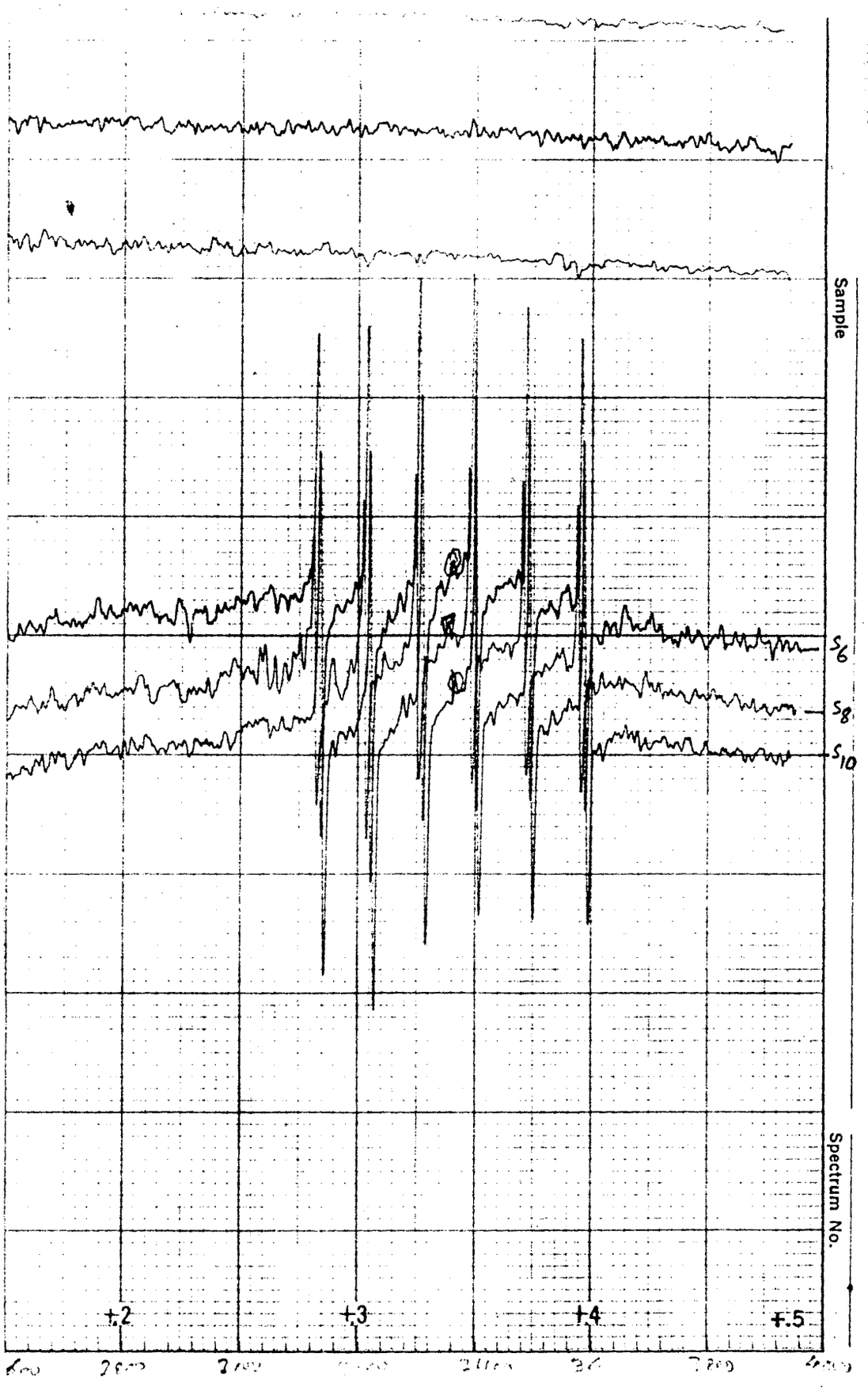

Fig. 4.6: EPR Spectra of fluxed CaO:Bi phosphors

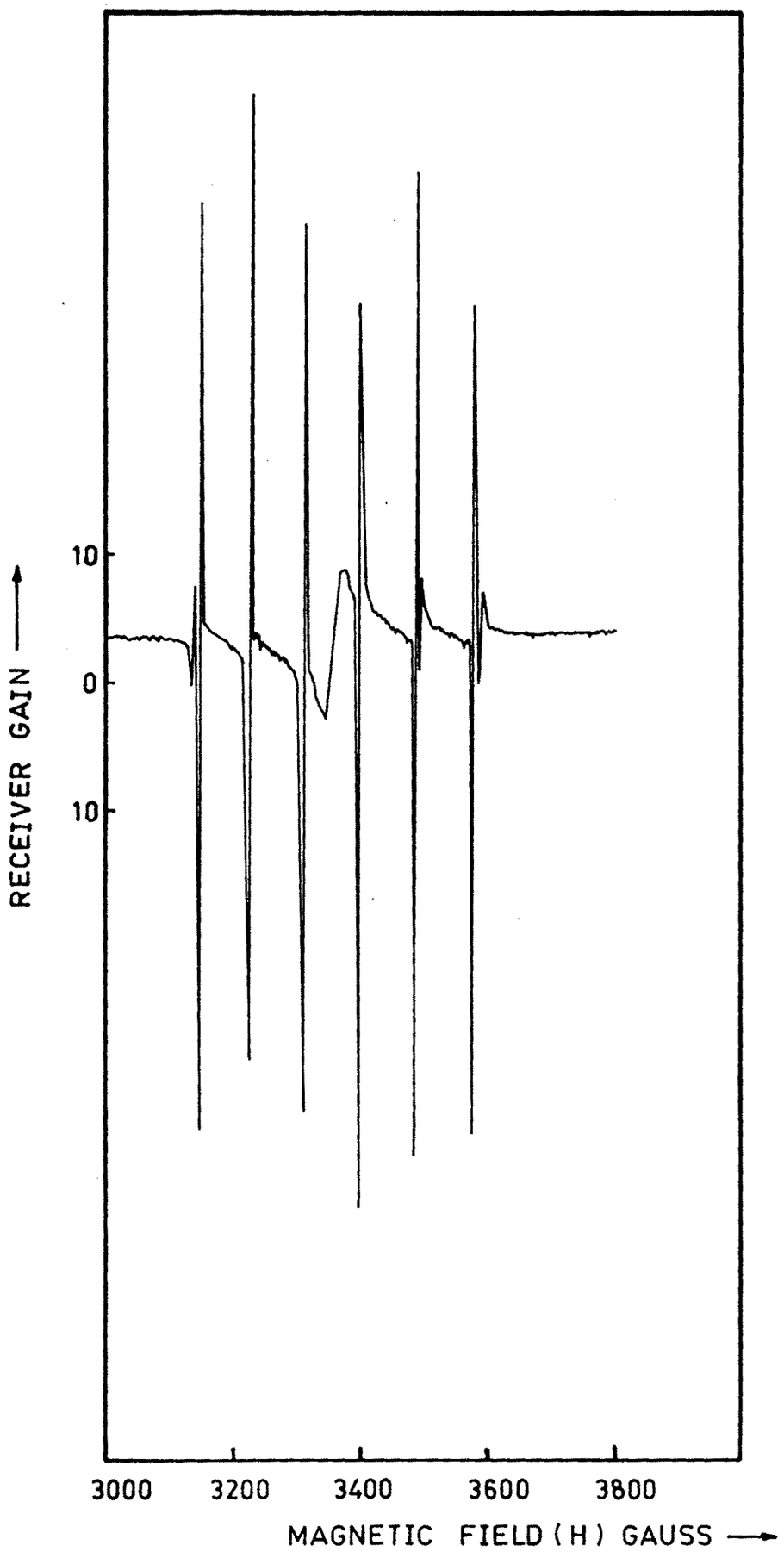

FIG. 4.7: EPR SPECTRA OF FLUXED CaO:Sm PHOSPHOR (S_{12})

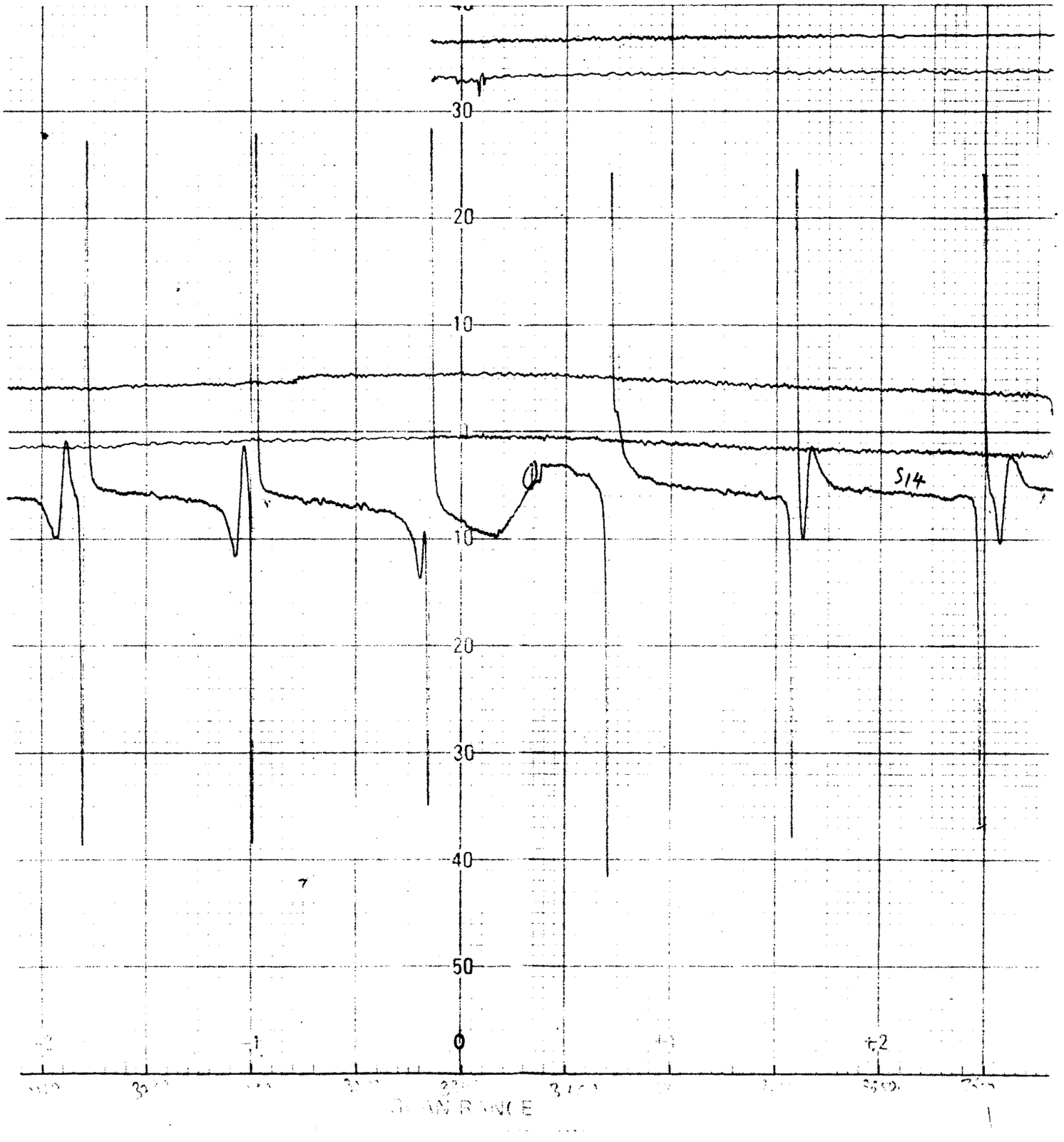

Fig. 4.7 EPR spectra of fluxed CaO:Sm phosphor(S14)

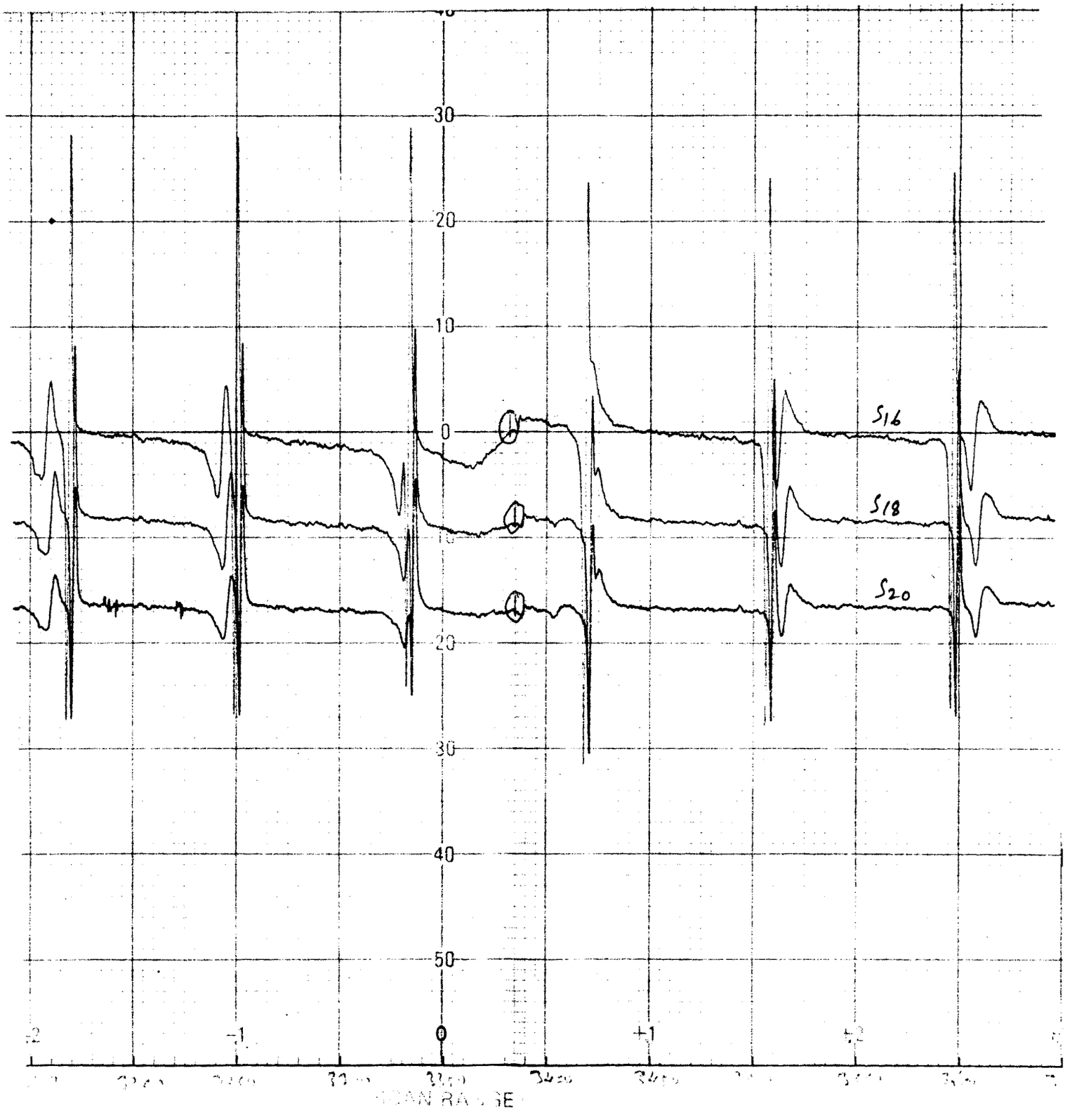

Fig. 4·8: EPR spectra of fluxed CaO:Sm phosphors

Fig. 4.9: EPR Spectra of fluxed CaO: Bi: Sm phosphor (S_{21})

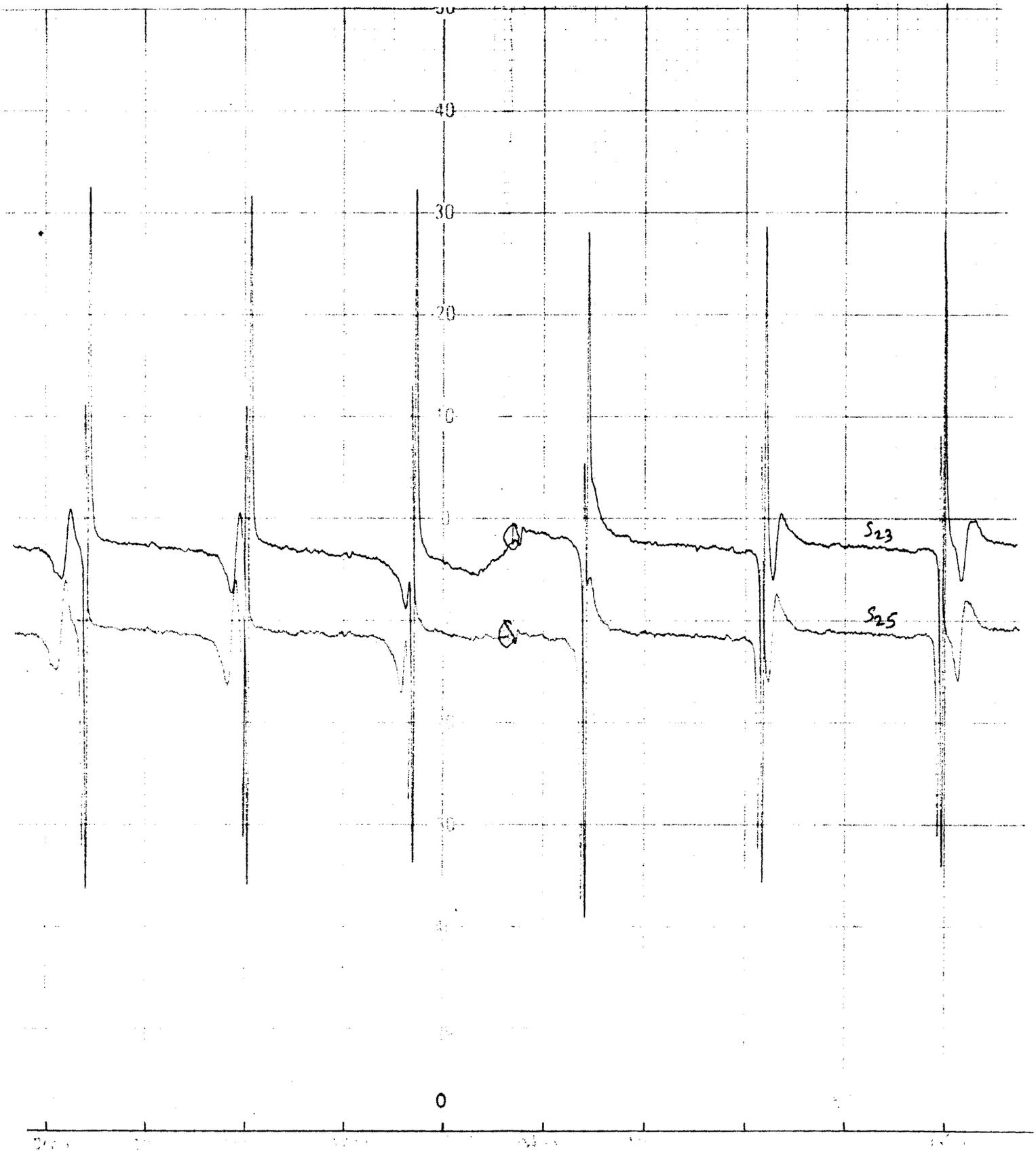

Fig. 4.10: EPR Spectra of fluxed CaO: Bi : Sm phosphors